Journal of
Synchrotron
Radiation

ISSN 0909-0495

addenda and errata

Two-dimensional approach to fluorescence yield XANES measurement using a silicon drift detector. Erratum

Y. Tamenori,[a]* M. Morita[b] and T. Nakamura[a]

[a]Japan Synchrotron Radiation Research Institute/SPring-8, 1-1-1 Kouto, Sayo 679-5198, Japan, and [b]Immunology Frontier Research Center, Osaka University, 3-1 Yamadaoka, Suita, Osaka 565-0871, Japan. E-mail: tamenori@spring8.or.jp

An error in the paper by Tamenori *et al.* [(2011), *J. Synchrotron Rad.* **18**, 747–752] is corrected.

In the second paragraph of §3.2 of Tamenori *et al.* (2011), we had provided incorrect fluorescence decay probability values for Mn L_{23}-shell ionization (0.0063) and O *K*-shell ionization (0.05). The correct fluorescence decay probability value of Mn L_{23}-shell ionization is 0.005 and that of O *K*-shell ionization is 0.0083 (Krause, 1979). Consequently, we had overestimated the difference between the fluorescence decay probabilities of Mn L_{23}-shell and O *K*-shell ionization.

Based on the correct fluorescence decay probability values, the Mn L_{23}-shell ionization value is about 60% of the O *K*-shell ionization value. This ratio supports a qualitative interpretation of the dip structure that appeared in the NEXAFS spectra of a MnO crystal [Fig. 3 of Tamenori*et al.* (2011)]. Furthermore, the model proposed in the original paper was also corroborated by two-dimensional fluorescence measurement results, which have been presented in the last paragraph of §3.2. Therefore, the overall conclusions of the original paper remain unchanged.

We thank Professor Toshiaki Ohta of Ritsumeikan University for drawing our attention to this error.

References

Krause, M. O. (1979). *J. Phys. Chem. Ref. Data*, **8**, 307–327.
Tamenori, Y., Morita, M. & Nakamura, T. (2011). *J. Synchrotron Rad.* **18**, 747–752.

  doi:10.1107/S0909049511041951

Journal of
Synchrotron Radiation

ISSN 0909-0495

Received 9 June 2011
Accepted 9 July 2011

Two-dimensional approach to fluorescence yield XANES measurement using a silicon drift detector

Y. Tamenori,[a]* M. Morita[b] and T. Nakamura[a]

[a]Japan Synchrotron Radiation Research Institute/SPring-8, 1-1-1 Kouto, Sayo 679-5198, Japan, and [b]Immunology Frontier Research Center, Osaka University, 3-1 Yamadaoka, Suita, Osaka 565-0871, Japan. E-mail: tamenori@spring8.or.jp

The objective of this article is to describe the capability of a two-dimensional (2D) approach to X-ray absorption near-edge structure (XANES) measurement by means of a partial fluorescence yield (PFY) method. 2D-XANES measurements were achieved by using a silicon drift detector as an energy-dispersive fluorescence detector. The advantage of this technique is that it allows full surveys of X-ray fluorescence data that are lost in conventional PFY measurements. The availability of a map approach was demonstrated by applying it to XANES measurements in both a diluted (Mn-doped nano-diamond) and a concentrated (MnO crystal) manganese sample. The 2D approach clearly distinguished between the PFY spectra of Mn and O atoms, where absorption edges of both elements are close to each other. Further, the 2D approach extracted an unambiguous PFY spectrum of phosphorus in the XANES measurement of SS304 ($P < 0.045$ wt%).

Keywords: XANES; soft X-rays; silicon drift detector; partial fluorescence yield; map approach.

1. Introduction

Since the pioneering work by Jaklevic *et al.* in 1977 (Jaklevic *et al.*, 1977), fluorescence yield (FY) detection has been widely used to measure X-ray absorption fine-structure (XAFS) spectra of dilute samples in the hard X-ray region. On the other hand, FY detection is not a mainstream technique in the soft X-ray region because fluorescence decay is a minor channel for low-Z elements (Krause, 1979). For example, the fluorescence decay probability for an oxygen 1s core-hole is less than 1%, in which case electron yield measurement is a common technique for obtaining the XANES spectrum in the soft X-ray region.

Although the yield of fluorescence decay is low, FY detection has unique advantages over electron yield detection. First, X-ray fluorescence has a much deeper escape depth than the electron. Therefore, simultaneous collection of both fluorescence and electron yield provides an opportunity to distinguish electronic properties between the surface and bulk of materials (Tröger *et al.*, 1990; Krol *et al.*, 1990; Stöhr, 1992). Second, the detection of FY is insensitive to sample charging, which makes it applicable for measuring the XAFS spectrum of insulating materials (Lipp *et al.*, 2003). Third, fluorescence measurement is possible under non-UHV conditions, allowing investigation of the materials under *in situ* conditions (Kappen *et al.,* 2001*a*, 2002; Yagi *et al.*, 2004; Nakanishi *et al.*, 2010). Fourth, FY detection is possible in a strong magnetic field, and it is applicable to magnetic circular dichroism measurements (Bateman *et al.*, 2001). Leveraging such advantages of fluorescence detection, a wide variety of applications using FY measurement in the soft X-ray region are being explored.

In addition to the above-mentioned advantages, the greatest characteristic of FY detection in XAFS measurement is a higher signal-to-background ratio than the transmission method and the electron yield detection method (Stöhr, 1992; Kappen *et al.*, 2002; Carlson *et al.*, 2006). This advantage allows us to measure low-concentration elements in chemical compounds. In the early stage of XAFS research, FY measurements were performed by total fluorescence detection using a non-energy-dispersive detector, *e.g.* a Lytle-type detector (Lytle *et al.*, 1984), a micro-channel plate or a silicon PIN photodiode detector. The detection sensitivity of the total fluorescence yield method is approximately 1% (Kappen *et al.*, 2002). An alternative approach is partial fluorescence detection which is possible by using an energy-dispersive detector such as a proportional counter (Fischer *et al.*, 1989), gas microstrip detector (Bateman *et al.*, 2001; Lipp *et al.*, 2003) or semiconductor detector. Using a silicon drift detector (SDD), which is a semiconductor detector, is the most widely applied method of XAFS measurement. The principle of the SDD was first proposed by Gatti & Rehak (Gatti & Rehak, 1984; Guazzoni, 2010), and is now commercially available. The SDD is unique because it achieves a higher energy resolution and higher count rate at shorter shaping times compared with conventional semiconductor detectors, and it can be used near room temperature (Lechner *et al.*, 1996; Lutz, 2006; Welter *et*

al., 2009). The high count rate of the SDD can compensate for low fluorescence yield in the soft X-ray region, and it can distinguish the fluorescence line of interest from the peak caused by elastic scattering and from neighbouring fluorescence lines. Selective X-ray fluorescence detection can improve the detection sensitivity, and XANES spectra have been obtained for elements with concentrations lower than 100 p.p.m. (Kappen *et al.*, 2002).

In the present research, we have introduced a two-dimensional (2D) approach for the partial fluorescence yield (PFY) measurement using a SDD in the soft X-ray region. The 2D measurement is a correlation plot between the excitation energy and the spectrum obtained by a secondary spectrometer. This technique has been developed in photoelectron spectroscopy combined with a hemispherical (Hikosaka *et al.*, 1996) and a time-of-flight analyzer (Berrah *et al.*, 1998), and in UVU fluorescence spectroscopy (Ukai *et al.*, 1995), and resonant inelastic X-ray scattering spectroscopy using a grating monochromator (Fuchs *et al.*, 2009). In X-ray fluorescence measurements the 2D approach can be achieved by using an energy-dispersive detector such as a SDD, since it can also produce a full X-ray fluorescence (XRF) spectrum.

The advantage of recording full XRF spectra in the fluorescence XAFS measurement is a more precise data treatment (Kappen *et al.*, 2001*b*; Mangold & Welter, 2001). In conventional procedures of PFY measurement the XRF information was lost because the PFY was collected by selecting a region of interest (ROI) prior to the XANES data collection. Only a signal corresponding to the ROI is recorded. This is problematic for PFY measurement of complicated samples in which overlaid peaks obscure the fluorescence (Kappen *et al.*, 2001*b*; Mangold & Welter, 2001). This issue is more serious in the soft X-ray region where absorption edges of different elements are close to each other and where fluorescence lines overlap. In such cases it is indispensable to store the entire fluorescence spectrum at every single point of the XAFS scan, and to validate the obtained spectrum after the XAFS measurement. In current procedures the highly brilliant soft X-ray beam and high-count-rate performance of an SDD allow us to collect complete 'X-ray fluorescence yield maps' instead of ROI data, even for low-concentration samples of less than 0.1 wt%. In the present report we will demonstrate the capabilities of the 2D map approach for partial fluorescence XANES measurements using an SDD detector in the soft X-ray region. The 2D approach allows us to obtain the correct PFY spectrum by surveying full XRF spectra prior to extracting the PFY spectrum.

2. Experimental

2.1. Beamline

Experiments were carried out at the c-branch of the soft X-ray photochemistry beamline (BL27SU) at the SPring-8 facility. Details of the beamline have been described in a previous report (Ohashi *et al.*, 2001). The light source was radiation from a figure-8 undulator, which can produce a linearly polarized photon beam (Tanaka *et al.*, 1998). The figure-8 undulator provides both horizontally and vertically polarized soft X-ray beams by selection of an appropriate undulator gap, with the linear electric vector lying horizontally (0°) for integer-order-harmonic light and vertically (90°) for half-integer-order light. The photon beam was dispersed by a soft X-ray monochromator with varied-line-spacing plane gratings. Two spherical mirrors and three gratings allow the scanning of an energy range of 170–2800 eV (Tamenori *et al.*, 2002). The XAFS spectra were measured by scanning the undulator gap as well as the monochromator scan to maintain the maximum intensity of the incident soft X-rays, and by scanning the width of the entrance and exit slits to maintain constant resolving power. During the XANES measurement the intensity of the incoming photon beam (I_0) was monitored by measuring a drain current on the surface of a post-focusing mirror.

2.2. SDD detector

The fluorescence signal was detected using a single-element SDD. The SDD used in the present investigation was purchased from OURSTEX Corporation (X Flash Detector, 1201 series). The active area of the photodetection element is 30 mm^2. The entrance window mounted on the front of the detector is a MOXTEK AP3.3 window consisting of ultra-thin polymer film (300 nm thick, density 1.4 g cm^{-3}) and is supported by a 38 µm-thick rigid silicon grid with 77% open area. The SDD module equipped with the AP3.3 window provides an X-ray transmission to the detector as low as the boron $K\alpha$ X-ray energy (170 eV), *i.e.* the detector is applicable to XANES experiments at the boron *K*-edge. The photodetection element is cooled down to 253 K using a Peltier device to avoid temperature noise from the field-effect transistor of a preamplifier. A KETEK digital pulse processor board (DPP) was used as a signal-processing unit. The SDD output is processed by a preamplifier, followed by an analog shaping amplifier. The output signal was digitized by an ADC/MCA and transferred to the onboard memory. The spectrum was transferred to the controlling computer through a USB 2.0 interface. The maximum count rate achieved by the SDD combined with the DPP system is 1×10^5 counts s^{-1} at 1 µs of peaking time.

2.3. XANES set-up

A powder sample was fixed with conductive double-sided carbon tape onto an aluminium sample holder. A solid sample was directly mounted on the sample plate using a screw. The sample holder was fixed on a linear and rotatable manipulator and installed in a vacuum chamber. The pressure of the XANES chamber was 1×10^{-5} Pa. The spectrum was recorded simultaneously in both total electron yields (TEYs) by measuring a sample drain current and FY spectra using a SDD. The SDD was mounted perpendicularly to the incident photon beam axis. The monochromatic light was irradiated at an angle of about 80° relative to the sample normal to minimize the contamination of the elastic scattering.

3. Results and discussion

3.1. XANES of phosphorus in SS304

The XANES spectrum of phosphorus in stainless steel (SS) 304 was measured using the 2D map approach. Generally, in SS304 samples, C (<0.08%), Mn (<2.0%), Si (<1.0%), P (<0.045%) *etc.* are present as minor components, while Cr (18–20%), Ni (8–10.5%) and Fe are present as major components. Fig. 1 shows (*a*) the 2D spectrum, (*b*) the XRF spectrum taken at 2190 eV and (*c*) the PFY spectrum extracted from the 2D spectrum. The XRF spectrum can be fitted well to seven Gaussian peaks, as indicated by lines (red online) in Fig. 1(*b*). The four peaks observed in the 400–1000 eV range originate from the *K*-shell ionization of oxygen and the L_{23}-shell ionization of the main elements, Cr, Fe and Ni. On the other hand, the fluorescence from Si and P *K*-shell ionization can be observed at approximately 1720 eV and 2000 eV, respectively. The interesting feature of these results is that the fluorescence counts of minor components are greatly enhanced in the XRF spectrum. For example, while the concentration of Fe is about 70 times larger than that of Si, the integrated fluorescence intensity of Si is approximately 50% of the intensity of Fe. There are three reasons for this phenomenon. First, the ionization cross section depends on the excitation energy. The ionization cross section reaches a maximum at an absorption edge and decreases with the increase of excitation photon energy. When an XRF spectra at 2 keV was obtained, the incident photon energy was approximately 1300 eV higher than the Fe L_{23} absorption edge and 300 eV above the Si *K*-edge, while the absorption coefficient of Si (3075.8 $cm^2\ g^{-1}$) at 2 keV was twice that of Fe (1665.8 $cm^2\ g^{-1}$) (Bandyopadhyay & Segre, undated). Second, the fluorescence decay probability following Si *K*-shell ionization (0.05) is about ten times larger than that of Fe L_{23}-shell ionization (0.0063) (Krause, 1979). Third, the transmission of the AP3.3 window for a 2000 eV photon (75%) is 1.5 times larger than that of a 700 eV photon (50%). Consequently, the fluorescence yields for minor elements are enhanced in the XRF measurement at 2 keV.

The FY from the main elements and Si make horizontal stripes in Fig. 1(*a*), because these elements have no absorption edges in this energy region. On the other hand, only the FY of phosphorous changes drastically. Fig. 1(*c*) shows the PFY spectrum extracted from integration of the 1940–2020 eV range. The obtained PFY spectrum closely resembles the XANES spectra of iron phosphate (Hesterberg *et al.*, 1999). While the XANES spectrum is clearly observed in the PFY mode, it cannot be found in the TEY spectrum (data not shown). In the TEY mode the imperceptible signals from the minor components are buried in the higher background signals originating from the excitation of major components, because Auger decay is the dominant decay channel following the *L*-shell ionization of 3*d* transition metals. The present measurement indicates that the selective fluorescence detection improves sensitivity to the imperceptible signal from phosphorus.

The patterns caused by elastic scattering appear as diagonal stripes in the 2D map. The energy of the phosphorus K_α (2013.7 eV) is about 30 eV lower than the binding energy of the phosphorus 1*s* electron (2045.5 eV). Therefore, the diagonal line does not directly intersect with the phosphorus K_α line in the XANES region. However, elastic scattering contributes to the baseline of the XANES spectrum. Fig. 2 compares the PFY spectra extracted from varying integration regions. This procedure corresponds to the PFY measurement with different ROI window selections. In principle, the baseline of the PFY spectrum should be flat in the pre-edge region, because the photon energy is insufficient to excite or ionize the P 1*s* electron and therefore cannot eliminate the K_α fluorescence from phosphorus. However, Fig. 2 shows that the baseline shape depends on the integrated area owing to the contamination of elastic scattering. The contamination is especially apparent when the higher fluorescence energy region is included in the PFY spectrum extraction as exhibited

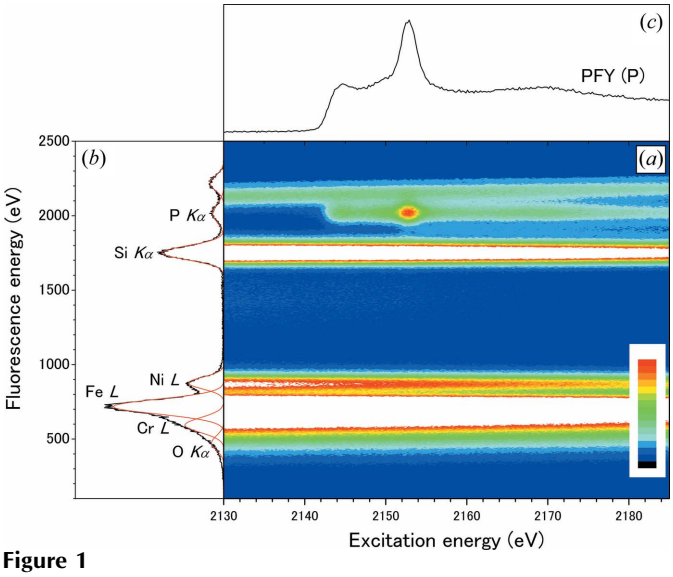

Figure 1
(*a*) Two-dimensional fluorescence spectrum for SS304 taken in the P *K*-edge region, (*b*) XRF spectrum taken at 2190 eV, and (*c*) PFY spectrum of phosphorus extracted from an integration of fluorescence counts in the range 1940–2020 eV.

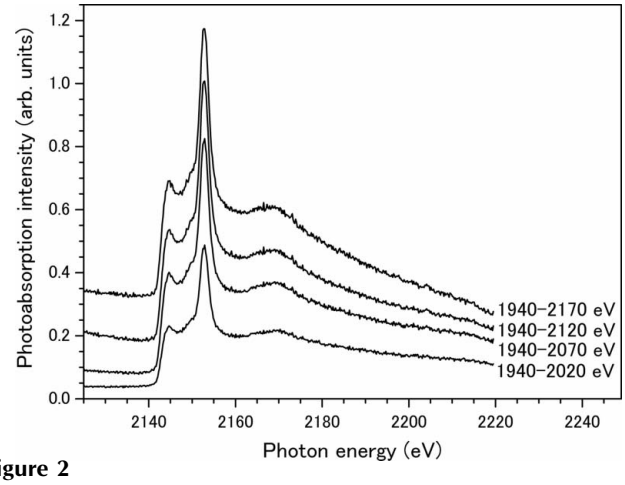

Figure 2
The extraction region dependence of the PFY spectrum of SS304 in the P *K*-edge region.

by the effect of the baseline in the pre-edge region and the tilt of the PFY baseline. This phenomenon could be a significant issue for subtraction of the baseline in the data analysis procedures of the EXAFS measurement. Recording of the full XRF is necessary for correct data treatment.

3.2. XANES of concentrated manganese: MnO crystal

Fig. 3 shows XANES spectra of a MnO crystal measured by (*a*) the total fluorescence yield (TFY) method and (*b*) the TEY method in the Mn L_{23}-edge region. The TEY spectrum presents two groups of multiplets split by the spin–orbit interaction of the Mn 2*p* inner-shell level. Here, it should be noted that the obtained TEY spectrum agrees well with the earlier reports on the oxidized MnO crystal (Gillbert *et al.*, 2003). It is well known that the TEY spectrum of MnO is sensitive to the surface condition (Gillbert *et al.*, 2003; Laffont & Gibot, 2010). In the present study we used a MnO crystal without surface cleaning such as cleaving and Ar ion sputtering, since the cleanness of the sample surface is not the essence of the present research. The surface of our MnO crystal was in a stable oxidized state, and can be confirmed from comparison with earlier reports.

On the other hand, the TFY spectra indicate different spectral profiles where the decrease in yield is observed at the L_3-edge and a weak peak is observed at the L_2-edge. The suppression of TFY at the absorption edge was observed in previous XANES investigations (Tröger *et al.*, 1990, 1992; Emura *et al.*, 1993). This phenomenon can be interpreted based on the change of the total photoabsorption coefficient and the change of fluorescence decay probabilities. Since the excitation energy of the L_{23}-edges of Mn (638.7 and 649.9 eV) is close to that of the O *K*-edge (543.1 eV), photoabsorption by both elements must be considered. The fluorescence intensity of the O K_α (I_O) is determined for a thick sample by the equation (Jaklevic *et al.*, 1977; Tröger *et al.*, 1990)

$$I_O \propto \varepsilon \frac{\mu_O(E)}{\mu_{tot}(E) + \mu_{tot}(E_{fl})} \quad (1)$$

where $\mu_{tot}(E)$ is the total photoabsorption coefficient of the sample at photon energy *E*, $\mu_O(E)$ is the absorption coefficient of the oxygen atom at photon energy *E*, $\mu_{tot}(E_{fl})$ is the photoabsorption coefficient at the fluorescence energy, and ε is the fluorescence decay probability of oxygen. Equation (1) suggests that the relative increase of $\mu_{tot}(E)$ leads to the decrease of the FY of oxygen. This can be understood as additional photoabsorption of manganese at the Mn L_{23}-edge leading to a reduction in the total number of photoexcited O atoms within the sample. On the other hand, even if the number of photoexcited O atoms is decreased, the TFY should be enhanced at the Mn L_{23}-edge if the fluorescence decay probability of manganese is comparable with that of oxygen. However, the fluorescence decay probability following the Mn L_{23}-shell ionization (0.0063) is about ten times smaller than that of the O *K*-shell ionization (0.05) (Krause, 1979). Therefore, the TFY spectrum indicates a dip profile at the Mn L_{23}-shell edges.

The above-mentioned interpretation can be confirmed by the 2D fluorescence measurement. Fig. 4(*a*) shows the 2D spectrum of MnO in the Mn L_{23}-edge region. The XRF spectrum (Fig. 4*b*) fits well to two Gaussian peaks, and the excitation energy dependence of the fluorescence signals from each element is well distinguished in the 2D map. Fig. 4(*c*) shows a PFY spectrum of oxygen (400–520 eV) and manganese (630–750 eV) extracted from the integration of fluorescence counts in the 2D spectrum. The decrease of the O K_α FY at the Mn L_{23}-edge is evidently confirmed in the PFY of oxygen. The PFY(O) indicates the inverted spectral profile to the TEY and PFY(Mn) spectrum. In contrast, the PFY of manganese indicates two groups of multiplets split by the spin–orbit interaction of the Mn 2*p* level. Compared with the TEY spectrum, the yield of the L_3-peak in PFY(Mn) is suppressed. The suppression could originate from self-absorption owing to the concentrated manganese in the sample. Consequently, the TFY shows strong suppression at the L_3-edge, while a small peak appears at the L_2-edge.

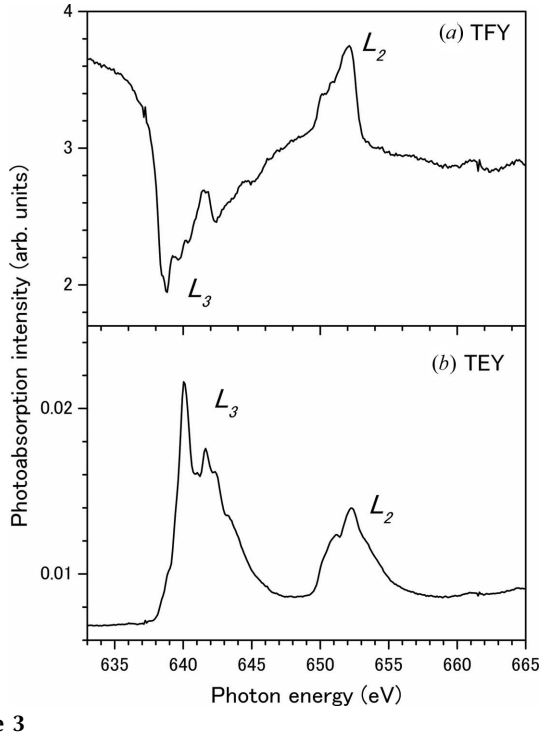

Figure 3
NEXAFS spectra of a MnO crystal measured by (*a*) the total fluorescence yield method and (*b*) the total electron yield method.

3.3. XANES of diluted manganese: manganese doped in nano-diamond

To verify the validity of the discussion in §3.2 we have measured the 2D spectrum of diluted manganese in the L_{23}-edge region. Fig. 5(*a*) shows the 2D spectrum of Mn (1×10^{16} cm^{-2}) doped in nano-diamond taken in the Mn L_{23}-edge region. The XRF spectrum (Fig. 5*b*) fits well to three Gaussian peaks. The peak at about 280 eV can be assigned to the K_α of carbon. The peak at 526.5 eV corresponds to the K_α of oxygen because a lot of water molecules are absorbed by the nano-

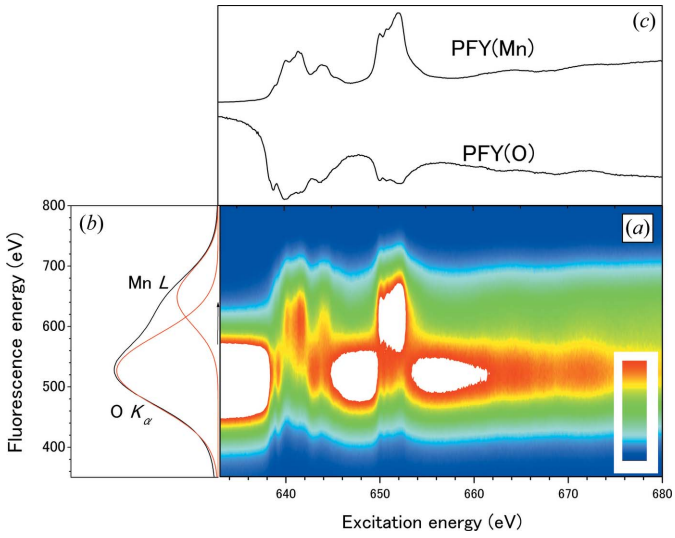

Figure 4
(*a*) Two-dimensional fluorescence spectrum for MnO crystal taken in the Mn L_{23}-edge region, (*b*) XRF spectrum taken at 680 eV, and (*c*) PFY spectrum of manganese and oxygen extracted from the 2D spectrum.

diamond. The peak at 648.1 eV corresponds to the *L*-line of manganese.

In Fig. 5(*a*) the two horizontal stripes observed at the fluorescence energies of 283.7 eV and 525.1 eV correspond to the K_α of carbon and the K_α of oxygen, respectively. Further, additional contour islands are noticeable on the horizontal line at 646.5 eV, corresponding to the resonant excitation of manganese. Fig. 5(*c*) shows the PFY spectrum of manganese extracted from an integration of fluorescence counts in the range 600–750 eV. The observed PFY spectrum is consistent with the XANES spectrum of Mn(II) (de Groot *et al.*, 1990). In contrast to the XANES measurement of the MnO crystal, the suppression of the K_α of oxygen and carbon is limited, because the concentration of manganese in the sample is low

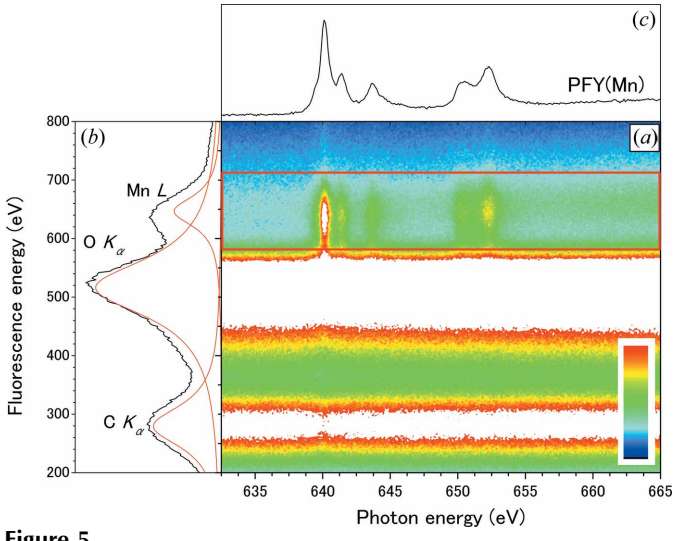

Figure 5
(*a*) Two-dimensional fluorescence spectrum for Mn-doped (1×10^{16} cm^{-2}) nano-diamond taken in the Mn L_{23}-edge region, (*b*) XRF spectrum taken at 640 eV, and (*c*) PFY spectrum of manganese extracted from the 2D spectrum.

and the change in $\mu_{tot}(E)$ at the Mn L_{23}-edge is small. Additionally, the self-absorption effect seems to be negligible owing to the low concentration of the investigated element.

The present results demonstrate the advantage of the 2D approach to PFY measurement where the FY of several elements is simultaneously changed. In conventional PFY measurement, users need to set the energy window prior to the incident photon energy scanning. Conversely, the 2D-map technique makes it possible to extract the partial fluorescence yield spectra after the incident photon energy scanning. This technique allows us to fully survey XRF spectra after the XAFS data collection, and to record the change in FY of all elements in the sample.

4. Summary

We have demonstrated the capabilities of a 2D approach to partial fluorescence yield XANES measurement using a silicon drift detector. The noteworthy advantage of 2D data collection is to allow a full survey of XRF spectra, and determine the extracting area after the XANES measurement. The availability was demonstrated using three XANES measurements. First, we obtained the PFY spectrum for a low-concentration element [P (<0.045%)] in an XANES measurement of SS304. By using a 2D technique we can verify the area where the PFY was extracted. Further, we performed the XANES measurement of manganese in both diluted and concentrated samples. In the case of the diluted sample, we extracted the PFY spectrum of manganese in the L_{23}-shell ionization region from Mn (1×10^{16} cm^{-2}) doped in nano-diamond. In the case of the concentrated sample the PFY of manganese indicates resonance peaks, whereas a strong suppression can be seen in the PFY of O atoms in the Mn L_{23}-edge region. The different behaviour of both elements can be interpreted based on the change of the total photoabsorption coefficient and the change of fluorescence decay probabilities. The 2D approach gives unambiguous FY-XANES information in the soft X-ray region, where absorption edges of different elements are close to each other, or where fluorescence lines overlap.

The authors would like to thank Mr M. Higashiyama for providing some of the key equipment used in this study. This study was conducted with the approval of the SPring-8 Proposal Review Committee (proposals 2009A2014, 2009B1999 and 2010A1104).

References

Bandyopadhyay, P. & Segre, C. U. (undated). *Mucal on the web*, http://www.csrri.iit.edu/mucal.html.
Bateman, J. E., Derbyshire, G. E., Dudzik, E., van der Laan, G., Lipp, J. D., Smith, A. D. & Stephenson, R. (2001). *J. Synchrotron Rad.* **8**, 1157–1161.
Berrah, N., Langer, B., Wills, A., Kukk, E. & Bozek, J. D. (1998). *Synchrotron Radiat. News*, **11**, 21–24.
Carlson, S., Clausén, M., Gridneva, L., Sommarin, B. & Svensson, C. (2006). *J. Synchrotron Rad.* **13**, 359–364.
De Groot, F. M. F., Fuggle, J. C., Thole, B. T. & Sawatzky, G. A. (1990). *Phys. Rev. B*, **42**, 5459–5468.

Emura, S., Moriga, T., Takizawa, J., Nomura, M., Bauchspiess, K. R., Murata, T., Harada, K. & Maeda, H. (1993). *Phys. Rev. B*, **47**, 6918–6930.
Fischer, D. A., Colbert, J. & Gland, G. L. (1989). *Rev. Sci. Instrum.* **60**, 1596–1602.
Fuchs, O., Weinhardt, L., Blum, M., Weigand, M., Umbach, E., Bär, M., Heske, C., Denlinger, J., Chuang, Y. D., McKinney, W., Hussain, Z., Gullikson, E., Jones, M., Batson, P., Nelles, B. & Follath, R. (2009). *Rev. Sci. Instrum.* **80**, 063103.
Gatti, E. & Rehak, P. (1984). *Nucl. Instrum. Methods Phys. Res.* **225**, 608–614.
Gillbert, B., Frazer, B. H., Belz, A., Conrad, P. G., Nealson, K. H., Haskel, D., Lang, J. C., Srajer, G. & De Stasio, G. (2003). *J. Phys. Chem. A*, **107**, 2839–2847.
Guazzoni, C. (2010). *Nucl. Instrum. Methods Phys. Res. A*, **624**, 247–254.
Hesterberg, D., Zhou, W., Hutchison, K. J., Beauchemin, S. & Sayers, D. E. (1999). *J. Synchrotron Rad.* **6**, 636–638.
Hikosaka, Y., Hattori, H., Hikida, T. & Mitsuke, K. (1996). *J. Chem. Phys.* **105**, 6367–6374.
Jaklevic, J., Kirby, J. A., Klein, M. P., Robertson, A. S., Brown, G. S. & Eisenberger, P. (1977). *Solid State Commun.* **23**, 679–682.
Kappen, P., Grunwaldt, J.-D., Clausen, B. S. & Materlik, G. (2001*b*). HASYLAB & DESY Annual Reports 2001, p. 5382. HASYLAB/DESY, Hamburg, Germany.
Kappen, P., Grunwaldt, J.-D., Hammershoi, B. S., Tröger, L. & Clausen, B. S. (2001*a*). *J. Catal.* **198**, 56–65.
Kappen, P., Tröger, L., Materlik, G., Reckleben, C., Hansen, K., Grunwaldt, J.-D. & Clausen, B. S. (2002). *J. Synchrotron Rad.* **9**, 246–253.
Krause, M. O. (1979). *J. Phys. Chem. Ref. Data*, **8**, 307–327.
Krol, A., Lin, C. S., Ming, Z. H., Sher, C. J., Kao, Y. H., Chen, C. T., Sette, F., Ma, Y., Smith, G. C., Zhu, Y. Z. & Shaw, D. T. (1990). *Phys. Rev. B*, **42**, 2635–2638.
Laffont, L. & Gibot, P. (2010). *Mater. Charact.* **61**, 1268–1273.
Lechner, P., Eckbauer, S., Hartmann, R., Krisch, S., Hauff, D., Richter, R., Soltau, H., Strüder, L., Fiorini, C., Gatti, El, Longoni, A. & Sampietro, M. (1996). *Nucl. Instrum. Methods Phys. Res. A*, **377**, 346–351.
Lipp, J. D., Bateman, J. E., Derbyshire, G. E., Kirkman, I. W., van der Laan, G., Stephenson, R. & Teodorescu, C. M. (2003). *J. Synchrotron Rad.* **10**, 455–460.
Lutz, G. (2006). *J. Synchrotron Rad.* **13**, 99–109.
Lytle, F. W., Greegor, R. B., Sandstrom, D. R., Marques, E. C., Wong, J., Spiro, C. L., Huffman, G. P. & Huggins, F. E. (1984). *Nucl. Instrum. Methods Phys. Res.* **226**, 542–548.
Mangold, S. & Welter, E. (2001). HASYLAB and DESY Annual Reports 2001, p. 5506. HASYLAB/DESY, Hamburg, Germany.
Nakanishi, K., Yagi, S. & Ohta, T. (2010). *AIP Conf. Proc.* **1234**, 931–934.
Ohashi, H., Ishiguro, E., Tamenori, Y., Kishimoto, H., Tanaka, M., Irie, M., Tanaka, T. & Ishikawa, T. (2001). *Nucl. Instrum. Methods Phys. Res. A*, **467**, 529–532.
Stöhr, J. (1992). *NEXAFS Spectroscopy*. Berlin: Springer.
Tamenori, Y., Ohashi, H., Ishiguro, E. & Ishikawa, T. (2002). *Rev. Sci. Instrum.* **73**, 1588–1590.
Tanaka, T., Maréchal, X.-M., Hara, T., Tanabe, T. & Kitamura, H. (1998). *J. Synchrotron Rad.* **5**, 459–461.
Tröger, L., Arvanitis, D., Baberschke, K., Michaelis, H., Grimm, U. & Zschech, E. (1992). *Phys. Rev. B*, **46**, 3283–3289.
Tröger, L., Arvanitis, D., Rabus, H., Wenzel, L. & Baberschke, K. (1990). *Phys. Rev. B*, **41**, 7297–7300.
Ukai, M., Machida, S., Kameta, K., Kitajima, M., Kouchi, N., Hatano, Y. & Ito, K. (1995). *Phys. Rev. Lett.* **74**, 239–242.
Welter, E., Hansen, K., Reckleben, C. & Diehl, I. (2009). *J. Synchrotron Rad.* **16**, 293–298.
Yagi, S., Matsumura, Y., Soda, K., Hashimoto, E. & Taniguchi, M. (2004). *Surf. Interface Anal.* **36**, 1064–1066.